

Vacuum-enhanced optical nonlinearities with organic molecular photoswitches

Marina Litinskaya^{1,*} and Felipe Herrera^{2,3,†}

¹*Department of Physics & Astronomy and Department of Chemistry,
University of British Columbia, Vancouver, Canada, V6T 1Z1*

²*Department of Physics, Universidad de Santiago de Chile, Av. Ecuador 3493, Santiago, Chile.*

³*Millennium Institute for Research in Optics MIRO, Chile.*

(Dated: April 6, 2018)

We propose a cavity QED scheme to enable cross-phase modulation between two arbitrarily weak classical fields in the optical domain, using organic molecular photoswitches as a disordered intracavity nonlinear medium. We show that a long-lived vibrational Raman coherence between the *cis* and *trans* isomer states of the photoswitch can be exploited to establish the phenomenon of vacuum-induced transparency (VIT) in high-quality microcavities. We exploit this result to derive an expression for the cross-phase modulation signal and demonstrate that it is possible to surpass the detection limit imposed by absorption losses, even in the presence of strong natural energetic and orientational disorder in the medium. Possible applications of the scheme include the development of organic nanophotonic devices for all-optical switching with low photon numbers.

Organic chromophores and semiconducting polymers are known for having very large optical nonlinearities [1], with applications in lasing [2], frequency conversion [3], nonlinear microscopy [4], and all-optical switching [5]. However, the typical magnitude of the nonlinear susceptibility in organic materials is still orders of magnitude below those needed to enable nonlinear optical effects at the level of single photons, an important prerequisite in photonic quantum technologies [6]. In recent years, the demonstration of strong and ultrastrong coupling of organic molecules with the quantized electromagnetic vacuum in optical and infrared cavities [7–10] has stimulated the study of single-photon control of chemical reactivity [11–13], energy transport [14, 15], charge transport [16, 17], and spectroscopy [18–21]. However, the manipulation of polariton coherences to enhance the natural optical nonlinearities of organic materials still remains a largely unexplored topic [22–24].

We propose a scheme to observe cross-phase modulation between two *arbitrarily weak* classical fields within a nanoscale cavity, using disordered organic molecular photoswitches as the intracavity medium. Molecular photoswitches are commonly used in photochemistry due to their ability to undergo spectrally-resolved photoisomerization processes [25], for applications such as optical information storage and controlled catalysis [26–28]. In this work, we suggest that natural features in the vibrational structure of organic photoswitches can be exploited to enable the observation of vacuum-induced transparency (VIT [29–32]), a variation of electromagnetically-induced transparency (EIT [33]) in which a cavity vacuum—rather than a strong control laser—is used to drive an internal coherence in the material. We further demonstrate that under conditions of VIT, the figure-of-merit for intracavity cross-phase mod-

ulation between the probe and signal fields can reach values that are orders of magnitude larger than without the cavity, exceeding the detection limit imposed by absorption losses. Replacing the control laser by a strongly coupled vacuum represents a clear advantage for organic materials with low laser damage thresholds [2]. Although EIT has been measured at low temperatures in solid state systems with negligible inhomogeneous broadening [34–37], condensed-phase VIT has yet to be demonstrated in systems with strong inhomogeneously broadening, such as organic molecular ensembles.

The envisioned light-matter scheme is shown in Fig. 1. The ground electronic potential of the photoswitch (S_0) has two deep wells in the isomerization coordinate corresponding to the *cis* and *trans* molecular isomers [25]. The lowest vibrational state of the *trans* isomer, is the stable ground state of the system $|1\rangle$. The meta-stable ground state $|2\rangle$ corresponds to the lowest vibrational level of the *cis* isomer potential well. Thermal isomerization of state

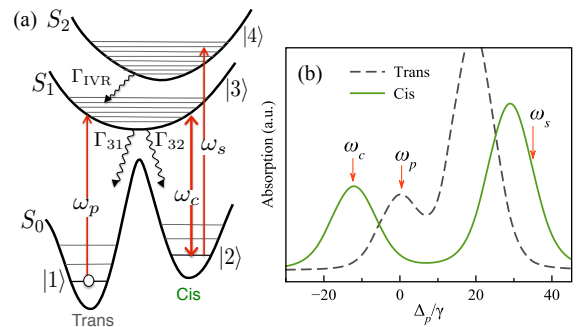


FIG. 1: Light-matter coupling scheme. (a) Energy level structure of molecular photoswitches. Straight arrows indicate near-resonant light-matter couplings at the cavity (ω_c), probe (ω_p) and signal (ω_s) frequencies. Curly arrows indicate non-radiative molecular decay processes. (b) Representative absorption spectrum of the molecular photoswitch. The highest *trans* absorption peak corresponds to the transition $S_0 \rightarrow S_2$.

*Electronic address: litinskaya@gmail.com

†Electronic address: felipe.herrera.u@usach.cl

|2⟩ is strongly suppressed [25], resulting in lifetimes for state |2⟩ of up to a few days at room-temperature [38, 39]. We associate the lowest two excited electronic potentials of the molecular photoswitch, S_1 and S_2 [40, 41], with the states |3⟩ and |4⟩, respectively. The vibrational structure of the excited potentials is not resolved in condensed phase, but S_0 has well-defined torsional modes with frequencies in the range $\omega_v \sim 160\text{--}190\text{ meV}/\hbar$ [42–44]. The level structure in Fig. 1 generalizes the atomic scheme introduced in Refs. [45, 46] to molecular systems with multiple ground state isomers.

Our model does not require an exact knowledge of the molecular potentials. Instead, we impose a set of constraints on the inhomogeneously-broadened photo-switch absorption spectrum outside the cavity, which we illustrate in Fig. 1b. We assume that the photo-switch spectrum has: (i) a well-resolved band associated with the *cis* transition $|2\rangle \rightarrow |3\rangle$, resonant with the cavity frequency ω_c ; (ii) a well-resolved band associated with the *trans* transition $|1\rangle \rightarrow |3\rangle$, near resonant with the probe frequency $\omega_p > \omega_c$; (iii) a well-resolved high-frequency band associated with the *cis* transition $|2\rangle \rightarrow |4\rangle$, weakly driven by a blue-detuned signal field at frequency $\omega_s > \omega_p$. These spectral requirements can be met using so-called *orthogonal* molecular photoswitches [47–49].

For a single molecular emitter, the light-matter coupling scheme in Fig. 1 can be modelled using the Hamiltonian

$$\begin{aligned} \hat{H}_S = & \omega_c \hat{a}^\dagger \hat{a} + \omega_{21} |2\rangle \langle 2| + \omega_{31} |3\rangle \langle 3| + \omega_{41} |4\rangle \langle 4| \\ & + \Omega_c (|3\rangle \langle 2| \hat{a} + |2\rangle \langle 3| \hat{a}^\dagger) + \Omega_p (|3\rangle \langle 1| e^{-i\omega_p t} \\ & + |1\rangle \langle 3| e^{i\omega_p t}) + \Omega_s (|4\rangle \langle 2| e^{-i\omega_s t} + |2\rangle \langle 4| e^{i\omega_s t}), \end{aligned} \quad (1)$$

where Ω_p and Ω_s are the probe and signal semiclassical Rabi frequencies, respectively. Ω_c is the cavity vacuum Rabi frequency, and \hat{a} is annihilation operator of the cavity field. In a dressed-state picture, our electronic basis must be supplemented with the cavity states to read: $|\bar{1}\rangle \equiv |1; 0_c\rangle$, $|\bar{2}\rangle \equiv |2; 1_c\rangle$, $|\bar{3}\rangle \equiv |3; 0_c\rangle$, and $|\bar{4}\rangle \equiv |4; 1_c\rangle$. The probe field thus drives the material transition $|\bar{1}\rangle \leftrightarrow |\bar{3}\rangle$, the signal field the transition $|\bar{2}\rangle \leftrightarrow |\bar{4}\rangle$, and the cavity field strongly admixes the nearly-degenerate dressed states $|\bar{2}\rangle$ and $|\bar{3}\rangle$.

We model energy disorder in the Hamiltonian \hat{H}_S by defining the random transition frequencies $\omega_{31} = \langle \omega_{31} \rangle + \delta_{31}$, $\omega_{32} = \langle \omega_{32} \rangle + \delta_{32}$ and $\omega_{42} = \langle \omega_{42} \rangle + \delta_{42}$, where $\langle \omega_{ji} \rangle$ corresponds to the band center frequency and δ_{ji} is a random static fluctuation that gives rise to the inhomogeneous linewidths σ_{ji} . Inhomogeneous linewidths due to energy disorder are typically in the range 150–200 meV for organic photoswitches [50], magnitudes that far exceed a typical homogeneous linewidth. In addition to energy disorder, below we also model orientational disorder in the system by writing the vacuum Rabi frequency as $\Omega_c = \Omega_0 \cos \theta$, where Ω_0 is a constant amplitude and θ is a uniformly distributed random angle between the molecular transition dipole moment and the space-fixed

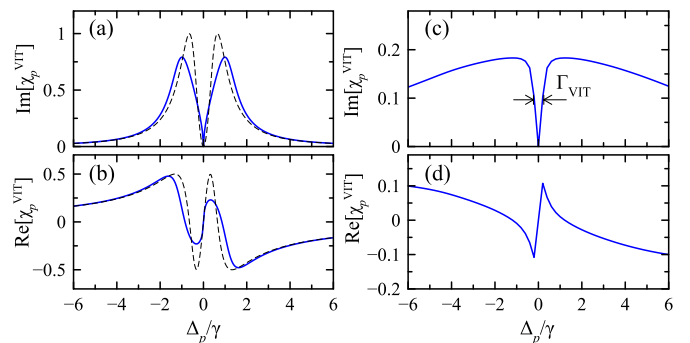


FIG. 2: Disorder-averaged absorptive ($\text{Im}\langle\chi_p^{\text{VIT}}\rangle$) and dispersive response ($\text{Re}\langle\chi_p^{\text{VIT}}\rangle$) of molecular photoswitches as a function of the probe detuning $\Delta_p = \omega_p - \langle\omega_{31}\rangle$, for a resonant cavity field $\omega_c = \langle\omega_{32}\rangle$. (a)-(b) Uniform orientational disorder on the vacuum Rabi frequency with mean amplitude $\Omega_0 = 1.2\gamma$. The disorder-free lineshape is shown for comparison (dashed line). (c)-(d) Gaussian disorder on ω_{31} for $\sigma = 6\gamma$ and $\Omega_c = 1.2\gamma$. The VIT linewidth Γ_{VIT} is graphically defined. γ is the homogeneous absorption linewidth.

cavity field polarization.

Although in general the dissipative dynamics of photoisomerization involves a complex interplay between non-adiabatic dynamics and non-secular relaxation [51, 52], in this work we adopt a simpler Lindblad quantum master equation approach to describe dissipation. We account for empty cavity decay with bare photon lifetimes assumed in the range $1/\kappa \sim 1 - 100$ ps, which can be achieved using high- Q dielectric cavities [53]. Non-radiative decay of the excited state $S_2 \rightarrow S_1$ by intramolecular vibrational relaxation (IVR) is also taken into account, with decay lifetime $1/\Gamma_{\text{IVR}} \sim 0.1$ ps [43], as well as non-radiative decay $S_1 \rightarrow S_0$ into the *trans* and *cis* ground states, at rates Γ_{31} and Γ_{32} , respectively. The homogeneous probe absorption linewidth is defined as $\gamma = \Gamma_{31} + \Gamma_{32}$, with typical excited state lifetimes in the range $1/\gamma \sim 0.1 - 0.5$ ps [50, 54]. Finally, we account for pure dephasing of the coherence between the vibrational ground states |1⟩ and |2⟩ at the rate Γ_{pd} , with typical dephasing times in range $1/\Gamma_{\text{pd}} \sim 1 - 100$ ps [55–58], depending on the molecular species, solvent and temperature. Having defined a master equation for the problem, we solve for the stationary reduced density matrix of the system to obtain an expression for disorder-free medium susceptibility at the probe frequency, denoted χ_p , to first order in Ω_p . The derivation can be found in the Supplemental Material (SM). We then obtain the disorder-averaged susceptibility $\langle\chi_p\rangle$, by integrating χ_p —both numerically and analytically—over random frequency configurations and dipole orientations. In what follows, we use the results of this procedure to describe the photo-physics of inhomogeneously broadened molecular photoswitches inside nanoscale optical cavities.

We begin our analysis of the intracavity response by assuming that no signal field is present ($\Omega_s = 0$). In Fig.

2, we show the corresponding disorder-averaged susceptibility $\langle \chi_p^{\text{VIT}} \rangle$ as a function of the mean probe detuning $\Delta_p \equiv \omega_p - \langle \omega_{31} \rangle$, for the representative decay ratios $\Gamma_{\text{pd}}/\gamma = 0.01$ and $\kappa/\gamma = 0.0001$. We numerically average the homogeneous response over a large number of disorder configurations, separately studying orientational disorder (panels a and b) and energy disorder (panels c and d). For energy disorder, we take the random frequency fluctuations δ_{ji} from independent Gaussian distributions with the same standard deviation, i.e. $\sigma_{ji} = \sigma$. We also assume that the cavity detuning $\Delta_c \equiv \omega_c - \langle \omega_{32} \rangle$ vanishes. Figure 2 clearly shows the characteristic signatures of VIT despite disorder: strong suppression of the probe absorption (transparency) and steep dispersion (slow light), over a narrow frequency window around two-photon resonance condition $\Delta_p - \Delta_c = 0$ [33]. Moreover, panels 2a-b show that uniform orientational disorder does not significantly alter the photoswitch response from the disorder-free case, reinforcing previous studies on the minor importance of orientational disorder in organic cavities [59], a result that can also be understood analytically (see SM for details).

Panels 2c,d show that even for strong inhomogeneous broadening due to energy disorder ($\sigma = 6\gamma$), a narrow VIT absorption dip with narrow linewidth Γ_{VIT} [60, 61] can still persist on top of a broader Gaussian absorption background, under two-photon resonance. For systems with arbitrary σ , which is the dominant energy scale in molecular photoswitches [50], we can achieve VIT as long as the frequency hierarchy $\kappa \sim \Gamma_{\text{pd}} \ll \Omega_c \lesssim \gamma$ holds. We find survival of VIT to inhomogeneous broadening under the assumption that the static energy fluctuations of states $|\tilde{1}\rangle$ and $|\tilde{2}\rangle$ are equal, i.e., $\delta_{31} = \delta_{32}$ to a very good approximation. The quality of VIT degrades as we allow the ground isomer potential minima to fluctuate independently. This sets a constraint on the contribution of inhomogeneous broadening on the vibrational Raman frequency ω_{21} to be much smaller than the excited state linewidth γ . If ω_{21} were to fluctuate significantly, the intracavity Raman dark state $|D\rangle = \sqrt{a}|\tilde{1}\rangle + \sqrt{1-a}|\tilde{2}\rangle$ ($0 < a < 1$), generated under VIT conditions [33], would rapidly dephase, breaking the destructive interference effect that causes the VIT absorption dip. However, given that both *cis* and *trans* isomers belong to the same electronic potential, it can be expected that $|\delta_{31} - \delta_{32}|/\gamma \ll 1$, independent of the molecular solvent.

Having established the physical conditions for achieving VIT in disordered molecular photoswitches, we now discuss a cross-Kerr scheme involving the simultaneous driving of the intracavity medium by both probe and signal fields. We focus on the phase shift Φ experienced by the probe field due to co-propagation with a signal field over a path length L . Attenuation at the probe frequency is quantified by the absorption coefficient α . Under conditions of VIT, both Φ and α not only depend on the probe and signal field frequencies and Rabi frequencies, but also on the cavity vacuum parameters [29, 30]. Following Ref. [62], we define the figure-of-

merit $\eta \equiv \Phi/\alpha L = \text{Re}\langle \chi_p \rangle / 2\text{Im}\langle \chi_p \rangle$ to quantify the degree by which it is possible to interferometrically resolve the nonlinear phase shift Φ at frequency ω_p . Detectable nonlinear signals require $\eta > 1$.

We developed an analytical approximation for the disorder-averaged susceptibility $\langle \chi_p \rangle$ in the presence of both probe and signal fields. We integrate the disorder-free susceptibility over the random fluctuations (δ_{31}, δ_{42}) assuming that they belong to independent Lorentzian distributions with different widths. We use Lorentzians instead of more realistic Gaussian distributions [44, 50] because the latter becomes analytically intractable for the cross-phase modulation signal that we seek to describe. Our approach is motivated by previous work on Doppler-broadened EIT [60, 61], and is justified below by comparison with a Gaussian numerical averaging. We show in the SM, that the mean susceptibility as a function of the probe detuning $x \equiv \Delta_p$ can be written in the form

$$2\langle \eta_p(x) \rangle = -\frac{x A_s(x) - \Omega_c^2(x - x_s)}{\Sigma_{31} A_s(x) + \Omega_c^2(\gamma_{21} + \gamma_s)}, \quad (2)$$

where $\gamma_{21} \equiv (\kappa/2 + \Gamma_{\text{pd}})$ is the decay rate of the coherence between dressed states $|\tilde{1}\rangle$ and $|\tilde{2}\rangle$. $\Sigma_{31} \equiv (\gamma/2 + \sigma_{31})$ is the total probe *trans* absorption linewidth, with σ_{31} being the inhomogeneous contribution. We have defined the function $A_s(x) \equiv (x - x_s)^2 + (\gamma_{21} + \gamma_s)^2$, characterized by the shift $x_s \equiv \lambda_s \Delta_s$ and the width $\gamma_s \equiv \lambda_s \Sigma_{41}$, written in terms of the dimensionless signal parameter

$$\lambda_s \equiv \Omega_s^2 / (\Delta_s^2 + \Sigma_{41}^2), \quad (3)$$

with $\Delta_s = \omega_s - \langle \omega_{42} \rangle$ being the mean signal detuning and $\Sigma_{41} \equiv \kappa/2 + \Gamma_{\text{IVR}}/2 + \sigma_{42}$, where σ_{42} is the inhomogeneous linewidth of the *cis* absorption band. Equation (2) shows that within our Lorentzian disorder model, the inhomogeneous linewidths σ_{31} and σ_{42} simply add up to the corresponding homogeneous linewidths, allowing for a transparent interpretation of the nonlinear system photophysics.

Outside the cavity ($\Omega_c = 0$), Eq. (2) simply reduces to the linear response result $\langle \eta_p \rangle = -\Delta_p/2\Sigma_{31}$, which near resonance gives $\langle \eta_p \rangle \ll 1$ due to the absorption of the probe. In the presence of the cavity vacuum, but without signal driving ($\Omega_s = 0$), the figure-of-merit $\langle \eta_p(\Omega_s = 0) \rangle \equiv \langle \eta_{\text{VIT}} \rangle$ can be considered as the degree of coherence in the response of the medium to the probe field. We show in the SM that in this VIT-regime, Eq. (2) reduces to

$$\langle \eta_{\text{VIT}}(x) \rangle \approx \frac{\Omega_c^2 x}{2(\Sigma_{31} x^2 + \gamma_{21} \Omega_c^2)} \gg 1, \quad (4)$$

under the conditions $\gamma_{21} \ll x \ll \Omega_c$. The large figure-of-merit predicted by Eq. (4) is a direct consequence of the transparency established for the probe field by the cavity vacuum.

For a system dominated by inhomogeneous broadening ($\gamma \ll \sigma_{31}$) inside a high- Q microcavity ($\kappa \ll \Gamma_{\text{pd}}$),

Eq. (4) has a maximum at the probe detuning $x_* = \Omega_c \sqrt{\Gamma_{\text{pd}}/\sigma_{31}}$, blue-shifted from the VIT absorption minimum, giving the optimal figure-of-merit

$$\langle \eta_{\text{VIT}}^{\text{max}} \rangle = \Omega_c / \sqrt{16 \Gamma_{\text{pd}} \sigma_{31}}. \quad (5)$$

With typical photoswitch parameters $\Gamma_{\text{pd}} \sim 1$ THz and $\sigma_{31} \sim 50$ THz, reaching $\langle \eta_{\text{VIT}}^{\text{max}} \rangle > 1$ would require $\Omega_c \geq 120$ meV. Vacuum Rabi frequencies of this order of magnitude and above can be obtained either by strongly confining the vacuum field to picoscale dimensions [63], or by exploiting collective Rabi coupling in larger cavities [53].

We next discuss the behaviour of Eq. (2) under simultaneous probe and signal driving ($\Omega_s > 0$). We refer to this as the VIT-Kerr regime, where the figure-of-merit is directly related with the magnitude of a cross-phase modulation signal [62]. Coupling to the signal field tends to destroy VIT, by weakly admixing the dark state $|D\rangle$ (see above), with the fast-decaying excited dressed state $|\tilde{4}\rangle$. The maximum achievable figure-of-merit $\langle \eta_{\text{max}} \rangle$ subject to signal driving therefore cannot exceed the VIT bound in Eq. (5), i.e., $\langle \eta_{\text{max}} \rangle \leq \langle \eta_{\text{VIT}}^{\text{max}} \rangle$ for any λ_s , with the equality sign holding only when $\lambda_s = 0$.

We can use Eq. (2) to find the constraints on x_s and γ_s that allow the nonlinear figure-of-merit to approach the VIT limit $\langle \eta_{\text{VIT}}^{\text{max}} \rangle$ (see SM for details). For instance, in realistic organic systems dominated by inhomogeneous broadening with $\Sigma_{41} \approx \Sigma_{31} \approx \sigma$ and assuming $\Omega_c/|\Delta_s| \leq \sqrt{\gamma_{21}/\sigma}$, our Lorentzian disorder model predicts that it is possible to reach $\langle \eta_{\text{max}} \rangle \gtrsim 1$ under a single constraint on the dimensionless signal parameter, given by

$$\lambda_s \lesssim \gamma_{21}/\sigma \ll 1. \quad (6)$$

Small values of λ_s are obtained by using weak signal fields, large (blue) signal detunings, or both.

We can now compare the predictions of our Lorentzian disorder model in Eq. (2) with a more realistic Gaussian model. Figure 3a shows the $\eta(x)$ -profiles predicted by the Lorentzian model and the result of numerically integrating over a large number of Gaussian configurations for δ_{31} and δ_{42} , again assuming that $\delta_{31} = \delta_{32}$ as in Fig. 2. We find that even when the Gaussian and Lorentzian noise distributions have equal widths (FWHM), Gaussian disorder consistently allows for higher values of $\langle \eta_{\text{max}} \rangle$. This behaviour is captured in panel 3b, which clearly shows that for our choice of material linewidths, a system with Gaussian disorder can surpass the limit $\langle \eta_{\text{max}} \rangle = 1$ for values of λ_s that are nearly an order of magnitude higher than those predicted by Eq. (6), which reduces the experimental constraints on the signal field. Figure 3b also shows that the Gaussian asymptote on $\langle \eta_{\text{max}} \rangle$ as $\lambda_s \rightarrow 0$, is about two times higher than the Lorentzian bound from Eq. (5). We also find that for values of λ_s of order 10^{-2} and above, the predictions of the Gaussian and Lorentzian disorder models become indistinguishable.

Finally, we note that the single-emitter Hamiltonian \hat{H}_S in Eq. (1) can be generalized to the many-particle

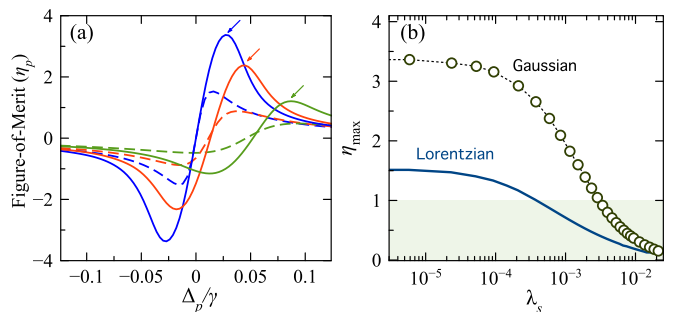


FIG. 3: Nonlinear figure-of-merit $\langle \eta_p \rangle$ for different signal parameters λ_s . (a) $\langle \eta_p \rangle$ as a function of probe detuning Δ_p for $\lambda_s = 0$ (blue line), $\lambda_s = 0.5$ (red) and $\lambda_s = 1$ (green). Solid curves correspond to a Gaussian disorder model and dashed lines to Lorentzian disorder. Arrows indicate the maximum figure-of-merit $\langle \eta_{\text{max}} \rangle$ for the Gaussian case. (b) $\langle \eta_{\text{max}} \rangle$ as a function of λ_s for Gaussian ($\sigma = 5\gamma$) and Lorentzian disorder distributions with equal width (FWHM). The shaded region corresponds to signal-to-noise ratios below unity for cross-phase modulation. In both panels we set $\gamma_{21} = 0.002\gamma$ and $\Omega_c = 0.8\gamma$.

case. In the regime where $\kappa < \sqrt{N}\Omega_c < \gamma$, we can replace one-body terms of the form $(\Omega_c |3_i\rangle \langle 2_i| \hat{a} + \text{H.c.})$ with the collective coupling term $(\sqrt{N}\Omega_c |\alpha_{cis}\rangle \langle G_{cis}| \hat{a} + \text{H.c.})$, where $|\alpha_{cis}\rangle = \sum_{i=1}^N |2_1, 2_2, \dots, 3_i, \dots, 2_N\rangle / \sqrt{N}$ is a totally-symmetric collective excitation [21], and $|G_{cis}\rangle \equiv |2_1, 2_2, \dots, 2_N\rangle$ is the *cis* ground state of the ensemble. The signal field thus weakly drives the coherence between the *cis* dressed ground state $|G_{cis}\rangle |1_c\rangle$ and state $|4_i\rangle |1_c\rangle$ on the *i*-th molecule. Our single-emitter results for $\langle \chi_p \rangle$ thus remain valid after replacing Ω_c by $\sqrt{N}\Omega_c$.

In summary, we propose an organic cavity scheme to achieve large cross-phase modulation signals using *arbitrarily weak* probe and signal fields. The scheme exploits a long-lived vibrational coherence between the *cis* and *trans* ground vibrational states in a class of chromophores known as molecular photoswitches, to establish conditions for vacuum-induced transparency inside high-*Q* optical microcavities. The predicted Kerr nonlinearity is found to exceed the corresponding cavity-free values by orders of magnitude, even in the presence of strong energy and orientational disorder in the organic medium. Our results may thus pave the way for the development of novel integrated nanophotonic devices for all-optical switching with narrow laser pulses at low power levels, using organic instead of inorganic materials [64] as the coherently driven nonlinear medium.

Acknowledgments

We thank Stéphane Kéna-Cohen and Yaroslav Ipolatov for comments. M.L. also thanks the Department of Physics at USACH for hospitality during early stages of this work. F.H. is supported by PAI 79140030, FONDECYT Iniciación 11140158,

- [1] Daniel Simon Chemla. *Nonlinear optical properties of organic molecules and crystals*, volume 1. Elsevier, 2012.
- [2] Alexander J. C. Kuehne and Malte C. Gather. Organic lasers: Recent developments on materials, device geometries, and fabrication techniques. *Chemical Reviews*, 116(21):12823–12864, 2016. PMID: 27501192.
- [3] Thierry Verbiest, Stephan Houbrechts, Martti Kauranen, Koen Clays, and Andre Persoons. Second-order nonlinear optical materials: recent advances in chromophore design. *J. Mater. Chem.*, 7:2175–2189, 1997.
- [4] Warren R Zipfel, Rebecca M Williams, and Watt W Webb. Nonlinear magic: multiphoton microscopy in the biosciences. *Nature Biotechnology*, 21:1369 EP –, 10 2003.
- [5] C. Koos, P. Vorreau, T. Vallaitis, P. Dumon, W. Bogaerts, R. Baets, B. Esembeson, I. Biaggio, T. Michinobu, F. Diederich, W. Freude, and J. Leuthold. All-optical high-speed signal processing with silicon–organic hybrid slot waveguides. *Nature Photonics*, 3:216 EP –, 03 2009.
- [6] Jeremy L. O’Brien, Akira Furusawa, and Jelena Vučković. Photonic quantum technologies. *Nature Photonics*, 3(12):687–695, December 2009.
- [7] D. G. Lidzey, D. D. C. Bradley, M. S. Skolnick, T. Virgili, S. Walker, and D. M. Whittaker. Strong exciton-photon coupling in an organic semiconductor microcavity. *Nature*, 395(6697):53–55, 09 1998.
- [8] Thomas W Ebbesen. Hybrid Light-Matter States in a Molecular and Material Science Perspective. *Accounts of Chemical Research*, 49:2403–2412, 2016.
- [9] Stéphane Kéna-Cohen, Stefan A. Maier, and Donal D. C. Bradley. Ultrastrongly coupled exciton–polaritons in metal-clad organic semiconductor microcavities. *Advanced Optical Materials*, 1(11):827–833, 2013.
- [10] J. P. Long and B. S. Simpkins. Coherent coupling between a molecular vibration and fabry–perot optical cavity to give hybridized states in the strong coupling limit. *ACS Photonics*, 2(1):130–136, 2015.
- [11] James A. Hutchison *et al.* Modifying chemical landscapes by coupling to vacuum fields. *Angew. Chem. Int. Ed.*, 51(7):1592–1596, 2012.
- [12] Felipe Herrera and Frank C. Spano. Cavity-controlled chemistry in molecular ensembles. *Phys. Rev. Lett.*, 116:238301, Jun 2016.
- [13] Javier Galego, Francisco J Garcia-Vidal, and Johannes Feist. Suppressing photochemical reactions with quantized light fields. *Nature Communications*, 7:13841, 2016.
- [14] J. Feist and F. J. Garcia-Vidal. Extraordinary exciton conductance induced by strong coupling. *Phys. Rev. Lett.*, 114:196402, 2015.
- [15] J. Schachenmayer, C. Genes, E. Tignone, and G. Pupillo. Cavity-enhanced transport of excitons. *Phys. Rev. Lett.*, 114:196403, 2015.
- [16] E. Orgiu *et al.* Conductivity in organic semiconductors hybridized with the vacuum field. *Nat Mater*, 14(11):1123–1129, 11 2015.
- [17] David Hagenmüller, Johannes Schachenmayer, Stefan Schütz, Claudiu Genes, and Guido Pupillo. Cavity-enhanced transport of charge. *Phys. Rev. Lett.*, 119:223601, Nov 2017.
- [18] Felipe Herrera and Frank C. Spano. Dark vibronic polaritons and the spectroscopy of organic microcavities. *Phys. Rev. Lett.*, 118:223601, May 2017.
- [19] Felipe Herrera and Frank C. Spano. Absorption and photoluminescence in organic cavity qed. *Phys. Rev. A*, 95:053867, May 2017.
- [20] Markus Kowalewski, Kochise Bennett, and Shaul Mukamel. Cavity femtochemistry; manipulating nonadiabatic dynamics at avoided crossings. *The journal of physical chemistry letters*, 2016.
- [21] Felipe Herrera and Frank C. Spano. Theory of nanoscale organic cavities: The essential role of vibration-photon dressed states. *ACS Photonics*, 5:65–79, 2018.
- [22] F. Herrera *et al.* Quantum nonlinear optics with polar J-aggregates in microcavities. *J. Phys. Chem. Lett.*, 5(21):3708–3715, 2014.
- [23] Bin Liu, Michael J. Crescimanno, and Kenneth D. Singer. Linear and nonlinear optical properties of organic cavity polaritons in the ultrastrong regime. In *Frontiers in Optics 2017*, page JTU3A.51. Optical Society of America, 2017.
- [24] Fábio Barachati, Janos Simon, Yulia A. Getmanenko, Stephen Barlow, Seth R. Marder, and Stéphane Kéna-Cohen. Tunable third-harmonic generation from polaritons in the ultrastrong coupling regime. *ACS Photonics*, 5(1):119–125, 2018.
- [25] Christophe Dugave and Luc Demange. Cis- trans isomerization of organic molecules and biomolecules: implications and applications. *Chemical reviews*, 103(7):2475–2532, 2003.
- [26] Jacques A. Delaire and Keitaro Nakatani. Linear and nonlinear optical properties of photochromic molecules and materials. *Chemical Reviews*, 100(5):1817–1846, 2000. PMID: 11777422.
- [27] Satoshi Kawata and Yoshimasa Kawata. Three-dimensional optical data storage using photochromic materials. *Chemical Reviews*, 100(5):1777–1788, 2000. PMID: 11777420.
- [28] RagnarS. Stoll and Stefan Hecht. Artificial light-gated catalyst systems. *Angewandte Chemie International Edition*, 49(30):5054–5075, 2010.
- [29] J. E. Field. Vacuum-rabi-splitting-induced transparency. *Phys. Rev. A*, 47:5064–5067, Jun 1993.
- [30] P.R. Rice and R.J Brecha. Cavity induced transparency. *Optics Communications*, 126(4):230 – 235, 1996.
- [31] Haruka Tanji-Suzuki, Wenlan Chen, Renate Landig, Jonathan Simon, and Vladan Vuletić. Vacuum-induced transparency. *Science*, 333(6047):1266–1269, 2011.
- [32] Martin Mücke, Eden Figueroa, Joerg Bochmann, Carolin Hahn, Karim Murr, Stephan Ritter, Celso J. Villas-Boas, and Gerhard Rempe. Electromagnetically induced transparency with single atoms in a cavity. *Nature*, 465(7299):755–758, 06 2010.
- [33] M. Fleischhauer, A. Imamoglu, and J. P. Marangos. Electromagnetically Induced Transparency: Optics in Coherent Media. *Rev. Mod. Phys.*, 77:633–673, Jul 2005.
- [34] B.S. Ham, P.R. Hemmer, and M.S. Shahriar. Efficient

- electromagnetically induced transparency in a rare-earth doped crystal. *Optics Communications*, 144(4):227 – 230, 1997.
- [35] Mark C. Phillips, Hailin Wang, I. Romyantsev, N. H. Kwong, R. Takayama, and R. Binder. Electromagnetically induced transparency in semiconductors via biexciton coherence. *Phys. Rev. Lett.*, 91:183602, Oct 2003.
- [36] Hailin Wang and Shannon O’Leary. Electromagnetically induced transparency from electron spin coherences in semiconductor quantum wells. *J. Opt. Soc. Am. B*, 29(2):A6–A16, Feb 2012.
- [37] V. M. Acosta, K. Jensen, C. Santori, D. Budker, and R. G. Beausoleil. Electromagnetically induced transparency in a diamond spin ensemble enables all-optical electromagnetic field sensing. *Phys. Rev. Lett.*, 110:213605, May 2013.
- [38] C. Barrett, A. Natansohn, and P. Rochon. Cis-trans thermal isomerization rates of bound and doped azobenzenes in a series of polymers. *Chemistry of Materials*, 7(5):899–903, 1995.
- [39] Jadranka Dokić, Marcel Gothe, Jonas Wirth, Maike V. Peters, Jutta Schwarz, Stefan Hecht, and Peter Saalfrank. Quantum chemical investigation of thermal cis-to-trans isomerization of azobenzene derivatives: Substituent effects, solvent effects, and comparison to experimental data. *The Journal of Physical Chemistry A*, 113(24):6763–6773, 2009. PMID: 19453149.
- [40] H. M. Dhammika Bandara and Shawn C. Burdette. Photoisomerization in different classes of azobenzene. *Chem. Soc. Rev.*, 41(5):1809–1825, 2012.
- [41] Eric M M Tan, Saeed Amirjalayer, Szymon Smolarek, Alexander Vdovin, Francesco Zerbetto, and Wybren Jan Buma. Fast photodynamics of azobenzene probed by scanning excited-state potential energy surfaces using slow spectroscopy. *Nature communications*, 6:5860, 2015.
- [42] D. R. Armstrong, J. Clarkson, and W. E. Smith. Vibrational Analysis of trans-Azobenzene. *The Journal of Physical Chemistry*, 99(51):17825–17831, 1995.
- [43] P. Hamm, S. M. Ohline, and W. Zinth. Vibrational cooling after ultrafast photoisomerization of azobenzene measured by femtosecond infrared spectroscopy. *The Journal of Chemical Physics*, 106(2):519–529, 1997.
- [44] Nandita Biswas, Becky Abraham, and Siva Umapathy. Investigation of short-time isomerization dynamics in p-nitroazobenzene from resonance Raman intensity analysis. *Journal of Physical Chemistry A*, 106(41):9397–9406, 2002.
- [45] H. Schmidt and A. Imamoglu. Giant kerr nonlinearities obtained by electromagnetically induced transparency. *Opt. Lett.*, 21(23):1936–1938, Dec 1996.
- [46] S. E. Harris and Y. Yamamoto. Photon switching by quantum interference. *Phys. Rev. Lett.*, 81:3611–3614, Oct 1998.
- [47] David Bléger, Jutta Schwarz, Albert M. Brouwer, and Stefan Hecht. o-fluoroazobenzenes as readily synthesized photoswitches offering nearly quantitative two-way isomerization with visible light. *Journal of the American Chemical Society*, 134(51):20597–20600, 2012. PMID: 23236950.
- [48] Claire E. Weston, Robert D. Richardson, Peter R. Haycock, Andrew J.P. White, and Matthew J. Fuchter. Arylazopyrazoles: Azoheteroarene photoswitches offering quantitative isomerization and long thermal half-lives. *Journal of the American Chemical Society*, 136(34):11878–11881, 2014.
- [49] Michael M. Lerch, Mickel J. Hansen, Willem A. Velema, Wiktor Szymanski, and Ben L. Feringa. Orthogonal photoswitching in a multifunctional molecular system. *Nature Communications*, 7(May):12054, 2016.
- [50] Christina M. Stuart, Renee R. Frontiera, and Richard A. Mathies. Excited-state structure and dynamics of cis- and trans-Azobenzene from resonance Raman intensity analysis. *Journal of Physical Chemistry A*, 111(48):12072–12080, 2007.
- [51] Birgit Balzer, Susanne Hahn, and Gerhard Stock. Mechanism of a photochemical funnel: A dissipative wavepacket dynamics study. *Chemical Physics Letters*, 379(3-4):351–358, 2003.
- [52] F. Rodriguez-Hernandez, A. Martinez-Mesa, and L. Uranga-Pina. Hybrid quantum-classical study of the non-adiabatic cis-trans photoisomerization in a model polyatomic molecule. *Chemical Physics Letters*, 592:18–23, 2014.
- [53] Denis G. Baranov, Martin Wersäll, Jorge Cuadra, Tomasz J. Antosiewicz, and Timur Shegai. Novel nanostructures and materials for strong light-matter interactions. *ACS Photonics*, 5:24–42, 2018.
- [54] Tatsuya Fujino, Sergei Yu. Arzhantsev, and Tahei Tahara. Femtosecond time-resolved fluorescence study of photoisomerization of trans-azobenzene. *The Journal of Physical Chemistry A*, 105(35):8123–8129, 2001.
- [55] Koichi Iwata, Ryosuke Ozawa, and Hiro-o Hamaguchi. Analysis of the solvent- and temperature-dependent raman spectral changes of s1 trans-stilbene and the mechanism of the trans to cis isomerization: dynamic polarization model of vibrational dephasing and the cc double-bond rotation. *The Journal of Physical Chemistry A*, 106(14):3614–3620, 2002.
- [56] Qing Hua Xu and M. D. Fayer. Temperature-dependent vibrational dephasing: Comparison of liquid and glassy solvents using frequency-selected vibrational echoes. *Journal of Chemical Physics*, 117(6):2732, 2002.
- [57] Andrew C. Terentis, Laszlo Ujj, Halina Abramczyk, and George H. Atkinson. Primary events in the bacteriorhodopsin photocycle: Torsional vibrational dephasing in the first excited electronic state. *Chemical Physics*, 313(1):51 – 62, 2005.
- [58] Masazumi Fujiwara, Kensei Yamauchi, Mitsuru Sugisaki, Andrew Gall, Bruno Robert, Richard J. Cogdell, and Hideki Hashimoto. Energy dissipation in the ground-state vibrational manifolds of β -carotene homologues: A sub-20-fs time-resolved transient grating spectroscopic study. *Phys. Rev. B*, 77:205118, May 2008.
- [59] Marina Litinskaya and Peter Reineker. Loss of coherence of exciton polaritons in inhomogeneous organic microcavities. *Phys. Rev. B*, 74:165320, Oct 2006.
- [60] Julio Gea-Banacloche, Yong-qing Li, Shao-zheng Jin, and Min Xiao. Electromagnetically Induced Transparency in Ladder-Type Inhomogeneously Broadened Media: Theory and Experiment. *Phys. Rev. A*, 51:576–584, Jan 1995.
- [61] Ali Javan, Olga Kocharovskaya, Hwang Lee, and Marlan Scully. Narrowing of electromagnetically induced transparency resonance in a Doppler-broadened medium. *Physical Review A*, 66(1):013805, jul 2002.
- [62] Hoonsoo Kang and Yifu Zhu. Observation of large kerr nonlinearity at low light intensities. *Phys. Rev. Lett.*, 91:093601, Aug 2003.
- [63] Rohit Chikkaraddy, Bart de Nijs, Felix Benz, Steven J.

Barrow, Oren A. Scherman, Edina Rosta, Angela Deme-
triadou, Peter Fox, Ortwin Hess, and Jeremy J. Baum-
berg. Single-molecule strong coupling at room tempera-
ture in plasmonic nanocavities. *Nature*, 535(7610):127–
130, 07 2016.

[64] Michael G. Moebius, Felipe Herrera, Sarah Griesse-

Nascimento, Orad Reshef, Christopher C. Evans,
Gian Giacomo Guerreschi, Alán Aspuru-Guzik, and Eric
Mazur. Efficient photon triplet generation in integrated
nanophotonic waveguides. *Opt. Express*, 24(9):9932–
9954, May 2016.

Appendix A: Derivation of the disorder-free susceptibility for organic photoswitches

1. Optical Bloch Equations for Cavity-Dressed States

We model the dynamics of the molecule-cavity reduced density matrix $\hat{\rho}_S$ by a quantum master equation of the form ($\hbar = 1$ throughout)

$$\frac{d}{dt}\hat{\rho} = -i[\hat{H}_S, \hat{\rho}_S] + \mathcal{L}_\kappa[\hat{\rho}] + \mathcal{L}_{S_2}[\hat{\rho}_S] + \mathcal{L}_{S_1}[\hat{\rho}_S] + \mathcal{D}_{\text{pd}}[\hat{\rho}_S] \quad (\text{A1})$$

where the Hamiltonian \hat{H}_S is given by Eq. (1) in the main text. The first dissipator in Eq. (A1) corresponds to cavity decay due to photon leakage into the far field at the rate κ , given by the Lindblad form

$$\mathcal{L}_\kappa[\hat{\rho}_S] = (\kappa/2) (2\hat{a}\hat{\rho}_S\hat{a}^\dagger - \hat{a}^\dagger\hat{a}\hat{\rho}_S - \hat{\rho}_S\hat{a}^\dagger\hat{a}), \quad (\text{A2})$$

The second dissipator represents the decay of the excited potential S_2 to S_1 via intramolecular vibrational relaxation (IVR) at the rate Γ_{IVR} , given by

$$\mathcal{L}_{S_2}[\hat{\rho}_S] = (\Gamma_{\text{IVR}}/2) (2|3\rangle\langle 4| \hat{\rho}_S |4\rangle\langle 3| - |4\rangle\langle 4| \hat{\rho}_S - \hat{\rho}_S |4\rangle\langle 4|) \quad (\text{A3})$$

The third dissipator represents non-radiative decay through a conical intersection followed by IVR, from the excited-potential S_1 to the *cis* and *trans* manifolds in the ground potential S_0 , given by

$$\begin{aligned} \mathcal{L}_{S_1}[\hat{\rho}_S] = & (\Gamma_{31}/2) (2|1\rangle\langle 3| \hat{\rho}_S |3\rangle\langle 1| - |3\rangle\langle 3| \hat{\rho}_S - \hat{\rho}_S |3\rangle\langle 3|) \\ & + (\Gamma_{32}/2) (2|2\rangle\langle 3| \hat{\rho}_S |3\rangle\langle 2| - |3\rangle\langle 3| \hat{\rho}_S - \hat{\rho}_S |3\rangle\langle 3|) \end{aligned} \quad (\text{A4})$$

We finally introduce an *ad-hoc* non-Lindblad term in Eq. (A1) to describe pure dephasing of the vibrational coherence between ground vibrational states in the *trans* and *cis* manifolds of S_0 at the rate Γ_{pd} , given by

$$\mathcal{D}_{\text{pd}}[\hat{\rho}_S] = -\Gamma_{\text{pd}} (|1\rangle\langle 1| \hat{\rho}_S |2\rangle\langle 2| + |2\rangle\langle 2| \hat{\rho}_S |1\rangle\langle 1|) \quad (\text{A5})$$

We neglect any contribution from the *cis*-to-*trans* thermal isomerization reaction in the master equation, given that the isomerization rate Γ_{21} is negligibly low in comparison with all other dynamical processes in the problem.

Before proceeding with the derivation of the probe susceptibility χ_p from the quantum master equation [Eq. (A1)], we introduce a convenient notation for the matrix elements of $\hat{\rho}_S$ that reads

$$\rho_{ij}^{mn}(t) = \langle i; m_c | \hat{\rho}(t) | j; n_c \rangle, \quad (\text{A6})$$

where $|i\rangle$ and $|j\rangle$ represent molecular states ($i, j = 1, 2, 3, 4$). $|m_c\rangle$ and $|n_c\rangle$ represent cavity Fock states with photon numbers m_c and n_c , respectively. We also define slowly-varying amplitudes for selected elements of reduced density matrix, to remove fast oscillations from the equations of motion. For the one-photon coherence $\rho_{13}^{00}(t)$, we define the slowly-varying amplitude $\sigma_{13}^{00}(t)$ by the relation $\sigma_{13}^{00} = \rho_{13}^{00} e^{-i\omega_p t}$. We also define the slowly-varying variables $\sigma_{12}^{01} = e^{-i\omega_p t} \rho_{12}^{01}$, $\sigma_{32}^{01} = \rho_{32}^{01}$, $\sigma_{14}^{01} = e^{-i(\omega_p + \omega_s)t} \rho_{14}^{01}$, $\sigma_{34}^{01} = e^{-i\omega_s t} \rho_{34}^{01}$, and $\sigma_{24}^{11} = e^{-i\omega_s t} \rho_{24}^{11}$. In terms of these slowly-varying amplitudes, we obtain from Eq. (A1) the following coherence equations of motion

$$\dot{\sigma}_{13}^{00} = i(\omega_{31} - \omega_p) \sigma_{13}^{00} - \gamma_{31} \sigma_{13}^{00} - i\Omega_p(\sigma_{33}^{00} - \sigma_{11}^{00}) + i\Omega_c \sigma_{12}^{01} \quad (\text{A7a})$$

$$\dot{\sigma}_{12}^{01} = i(\omega_{21} + \omega_c - \omega_p) \sigma_{12}^{01} - \gamma_{21} \sigma_{12}^{01} - i\Omega_p \sigma_{32}^{01} + i\Omega_c \sigma_{13}^{00} + i\Omega_s \sigma_{14}^{01} \quad (\text{A7b})$$

$$\dot{\sigma}_{32}^{01} = -i(\omega_{32} - \omega_c) \sigma_{32}^{01} - \gamma_{32} \sigma_{32}^{01} - i\Omega_c(\sigma_{22}^{11} - \sigma_{33}^{00}) - i\Omega_p \sigma_{12}^{01} + i\Omega_s \sigma_{34}^{01} \quad (\text{A7c})$$

$$\dot{\sigma}_{14}^{01} = i(\omega_{41} + \omega_c - \omega_p - \omega_s) \sigma_{14}^{01} - \gamma_{41} \sigma_{14}^{01} - i\Omega_p \sigma_{34}^{01} + i\Omega_s \sigma_{12}^{01} \quad (\text{A7d})$$

$$\dot{\sigma}_{34}^{01} = i(\omega_{43} + \omega_c - \omega_s) \sigma_{34}^{01} - \gamma_{43} \sigma_{34}^{01} - i\Omega_p \sigma_{14}^{01} - i\Omega_c \sigma_{24}^{11} + i\Omega_s \sigma_{32}^{01} \quad (\text{A7e})$$

$$\dot{\sigma}_{24}^{11} = i(\omega_{42} - \omega_s) \sigma_{24}^{11} - \gamma_{42} \sigma_{24}^{11} - i\Omega_c \sigma_{34}^{01} + i\Omega_s(\sigma_{22}^{11} - \sigma_{44}^{11}) \quad (\text{A7f})$$

where we introduce the decay rates

$$\gamma_{31} = \Gamma_{31}/2 + \Gamma_{32}/2 \equiv \gamma/2 \quad (\text{A8a})$$

$$\gamma_{21} = \kappa/2 + \Gamma_{\text{pd}} \quad (\text{A8b})$$

$$\gamma_{32} = \kappa/2 + \Gamma_{31}/2 + \Gamma_{32}/2 \quad (\text{A8c})$$

$$\gamma_{43} = \kappa/2 + \Gamma_{\text{IVR}}/2 \quad (\text{A8d})$$

$$\gamma_{42} = \kappa + \gamma_{\text{IVR}}/2 \quad (\text{A8e})$$

$$\gamma_{41} = \gamma_{43}. \quad (\text{A8f})$$

Equations (A8a) and (A8b) define the homogeneous probe and Raman linewidths γ and γ_{21} , in the notation from the main text. The vibrational pure dephasing rate Γ_{pd} determines the cavity-dressed Raman lifetime $1/\gamma_{21}$ for high- Q cavities with $\kappa \ll \gamma$.

In deriving Eqs. (A7a)-(A7f), we neglect the contribution of states such as $|2, 0_c\rangle$, $|3, 1_c\rangle$, or $|4, 0_c\rangle$, which are neither populated nor driven under our imposed assumptions of stationarity and weak signal and probe driving. Accounting for such states would result, for example, in the addition of an extra term proportional to σ_{13}^{11} in the right-hand side of equation (A7a) for $\dot{\sigma}_{13}^{00}$, term that can be shown to vanish in the stationary limit. In other words, the set of Eqs. (A7a-f) do not correspond to a complete description of the system coherences, but can be considered as a minimal set of equations of motion that can account for the non-linear optical response of our system of interest.

2. Homogeneously-broadened intracavity susceptibility

We look for the stationary one-photon probe coherence σ_{13}^{00} from Eqs. (A7). The medium polarization at the probe frequency is then given by $P(\omega_p) = d_{13}\sigma_{31}^{00}$, from semiclassical closure. Using $\Omega_p = -d_{31}E_p/2\hbar$ and $P(\omega_p) = \chi_p E_p$, the probe susceptibility χ_p for homogeneously-broadened organic molecular photoswitches can be written as

$$\chi_p = \frac{K}{(\Delta_{31} + I'_0) + i(\gamma_{31} + I''_0)}, \quad (\text{A9})$$

where $K = -|d_{13}^2|/2\hbar$ is proportional to the oscillator strength of the cavity-free probe absorption peak, $\Delta_{31} = \omega_p - \omega_{31}$ is the probe detuning from the *trans* transition. In the main text we use the notation $\Delta_{31} \equiv \Delta_p$.

In Eq. (A9), we have introduced the complex nonlinear quantity $I_0 \equiv I'_0 + iI''_0$, given by

$$I_0 = \frac{\Omega_c^2(\Delta_{41} + i\gamma_{41})(i\gamma_{32} - \Delta_{32})}{(i\gamma_{32} - \Delta_{32})\Omega_s^2 + (\Delta_{41} + i\gamma_{41})\Omega_p^2 - (\Delta_{21} + i\gamma_{21})(\Delta_{41} + i\gamma_{41})(i\gamma_{32} - \Delta_{32})}, \quad (\text{A10})$$

where $\Delta_{32} = \omega_c - \omega_{32}$ is the cavity detuning from the *cis* absorption resonance, $\Delta_{21} = \omega_p - \omega_c - \omega_{21}$ is the two-photon (Raman) detuning, and $\Delta_{41} = \omega_p - \omega_c + \omega_s - \omega_{41}$ is the three-photon detuning. The term in the denominator proportional to Ω_p^2 describes self-induced transparency, and is negligibly small in low- Ω_p limit. In what follows we use a simplified formula

$$I_0 = \frac{\Omega_c^2(\Delta_{41} + i\gamma_{41})}{\Omega_s^2 - (\Delta_{21} + i\gamma_{21})(\Delta_{41} + i\gamma_{41})}. \quad (\text{A11})$$

By setting $\Omega_s = 0$ in Eq. (A11), the susceptibility χ_p in Eq. (A9) reduces to the standard VIT form [29, 30]

$$\chi_p^{\text{VIT}} = \frac{K(\Delta_{21} + i\gamma_{21})}{(\Delta_{31} + i\gamma_{31})(\Delta_{21} + i\gamma_{21}) - \Omega_c^2}. \quad (\text{A12})$$

For later convenience, we introduce the dimensionless parameter

$$\lambda_c = \frac{\Omega_c^2}{(\Delta_{21}^2 + \gamma_{21}^2)}, \quad (\text{A13})$$

to rewrite Eq. (A12) as

$$\chi_p^{\text{VIT}} = \frac{K}{(\Delta_{31} - \lambda_c \Delta_{21}) + i(\gamma_{31} + \lambda_c \gamma_{21})}. \quad (\text{A14})$$

Appendix B: Derivation of $\langle \chi_p^{\text{VIT}} \rangle$ for disordered photoswitches without signal driving

In this Appendix, we derive expressions for the intracavity mean probe susceptibility $\langle \chi_p^{\text{VIT}} \rangle$, separately averaged over orientational and energy disorder in the organic photoswitch medium.

1. VIT with orientational disorder

For an organic system with orientational disorder, disorder average can be carried out by an integration of the form $\langle \chi_p^{\text{VIT}} \rangle_\theta = \int_{-\pi/2}^{\pi/2} d\theta \chi_p^{\text{VIT}}(\cos \theta) P(\theta)$, where χ_p^{VIT} is the uniform susceptibility given by Eq. (A12), and $P(\theta) = 1/2\pi$, with $-\pi/2 \leq \theta \leq \pi/2$ is a uniform distribution for the molecular *cis* transition dipole moment with respect to the cavity field polarization. By writing the vacuum Rabi frequency as $\Omega_c(\theta) = \Omega_0 \cos \theta$, we can express the mean susceptibility $\langle \chi_p^{\text{VIT}} \rangle_\theta$ as

$$\begin{aligned} \langle \chi_p^{\text{VIT}} \rangle_\theta &= K(\Delta_{21} + i\gamma_{21}) \frac{1}{2\pi} \int_0^{2\pi} \frac{d\theta}{\cos^2 \theta - (Z_1 + iZ_2)}, \\ &= K(\Delta_{21} + i\gamma_{21}) \frac{i \operatorname{sgn}(Z_2)}{\sqrt{(Z_1 + iZ_2)(1 - (Z_1 + iZ_2))}} \end{aligned} \quad (\text{B1})$$

where $Z_1 = (\Delta_{31}\Delta_{21} - \gamma_{31}\gamma_{21})/\Omega_0^2$ and $Z_2 = (\Delta_{31}\gamma_{21} + \Delta_{21}\gamma_{31})/\Omega_0^2$. Assuming for simplicity that $\gamma_{21} = 0$ and rearranging terms, we arrive at the expression

$$\langle \chi_p^{\text{VIT}} \rangle_\theta \equiv -K \frac{|\Delta_{21}|}{\sqrt{2}} \left[\frac{B + i(A + \Omega)}{\Omega \sqrt{A + \Omega}} \right], \quad (\text{B2})$$

where we have defined $A = \Delta_{21} [\Delta_{31}(\Omega_0^2 - \Delta_{21}\Delta_{31}) + \Delta_{21}\gamma_{31}^2]$, $B = \Delta_{21}\gamma_{31}(\Omega_0^2 - 2\Delta_{21}\Delta_{31})$, and $\Omega = \sqrt{A^2 + B^2}$. Equation (B2) is exact within the assumptions involved in Eqs. (A7a)-(A7f), and has excellent agreement with the numerical integration of Eq. (A9) over a large number of angular disorder configurations, as shown in Figure B.1a. The comparison of the VIT linewidth Γ_{VIT} for a system with orientational disorder and the disorder-free case in panel B.1b demonstrates the fluctuations of the dipole orientation preserves the linear scaling $\Gamma_{\text{VIT}} \sim \Omega_c$ characteristic of homogeneously-broadened EIT [1,2], but with a higher slope.

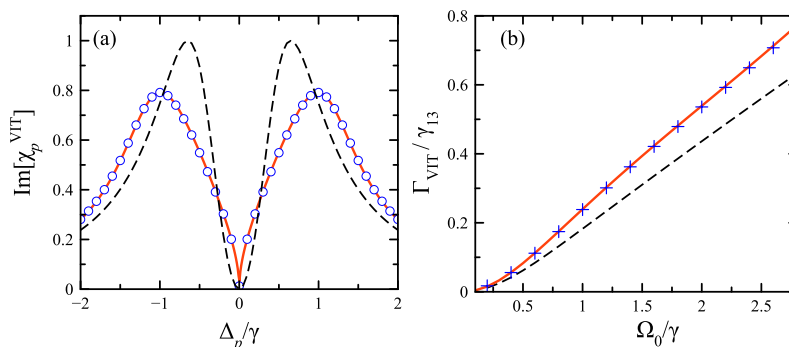


FIG. B.1: VIT lineshape for uniform orientational disorder. (a) Average $\text{Im}[\langle \chi_p^{\text{VIT}} \rangle]$ as a function of probe detuning Δ_p for $\Omega_0 = 1.2\gamma$. Solid line corresponds to the analytically expression in Eq. (B2), and circles correspond to numerical integration over a large number of disorder configurations. The homogeneous susceptibility is also shown for comparison (dashed line). (b) Scaling of the VIT linewidth Γ_{VIT} with the Rabi amplitude Ω_0 , obtained both analytically (solid line) and numerically (crosses). The homogeneous scaling is also shown for comparison (dashed line).

2. VIT with energy disorder

We average (A14) over energy disorder, by writing $\Delta_{31} = \langle \Delta_{31} \rangle + \delta_{31}$, and integrating over a Lorentzian distribution of the energy fluctuation given by $P(\delta_{31}) = \sigma_3/[\pi(\delta_{31}^2 + \sigma_3^2)]$, with σ_3 being the width of the energy (detuning)

distribution. Note that our assumption of correlated energy fluctuations of the states $|1\rangle$ and $|2\rangle$ implies that $\Delta_{21} = \omega_p - \omega_c - \omega_{21}$ is a well-defined quantity that does not fluctuate over the molecular ensemble. The resulting integral has one pole ($z = i\sigma_3$) in the upper half of the complex plane. The pole arising from the denominator of χ_p^{VIT} in Eq. (A14) always lays in the lower half-plane. We calculate the integral by closing the integration path in the upper half-plane and applying Cauchy's theorem. The result gives

$$\langle \chi_p^{\text{VIT}} \rangle_E = \frac{K}{(\Delta_{31} - \lambda_c \Delta_{21}) + i(\Sigma_{31} + \lambda_c \gamma_{21})}, \quad (\text{B3})$$

where we have defined the combined linewidth $\Sigma_{31} = \gamma_{31} + \sigma_3$. Comparing this result with the homogeneous susceptibility in Eq. (A14) we see that the energy disorder average with static ω_{21} results in an additive contribution to the probe transition linewidth given by σ_3 . This explains the survival of VIT conditional on the smallness of γ_{21} and the fact that it is not sensitive to the decay rate γ_{31} , which is eliminated by the opening of the transparency window.

The analytical expression in Eq. (B3) is in qualitative agreement with the results in Figure 2c,d, which were obtained numerically by averaging Eq. (A12) over a large number of detuning configurations δ_{31} , distributed according to a Gaussian probability density. Small quantitative discrepancies arise due to the difference between Gaussian and Lorentzian distributions. Gaussian distributions are more relevant for the energy disorder than Lorentzians. However, analytically averaging Eq. (A12) over a Gaussian distribution results in a much less intuitive answer than our result in Eq. (B3), in terms of integral special functions. Our Lorentzian ansatz can thus also provide a reasonably accurate description of the system response.

Appendix C: Derivation of $\langle \chi_p \rangle$ for photoswitches with energy disorder

Starting from the expression for the disorder-free susceptibility in Eq. (A9), with I_0 as given in Eq. (A11), we introduce the random transition frequencies $\omega_{31} = \langle \omega_{31} \rangle - \delta_{31}$, $\omega_{32} = \langle \omega_{32} \rangle - \delta_{32}$, and $\omega_{42} = \langle \omega_{42} \rangle - \delta_{42}$, where $\langle \omega \rangle$ represents a mean value and δ a random static fluctuation described by the normalized distribution function $P(\delta)$. These random frequencies give rise to the random detunings $\Delta_{31} \equiv \omega_p - \langle \omega_{31} \rangle + \delta_{31} = \langle \Delta_{31} \rangle + \delta_{31}$ and $\Delta_{41} \equiv \omega_p - \omega_c + \omega_s - (\langle \omega_{42} \rangle - \delta_{42} - \langle \omega_{32} \rangle + \delta_{32} + \langle \omega_{31} \rangle - \delta_{31}) = \langle \Delta_{41} \rangle + (\delta_{42} - \delta_{32} + \delta_{31})$, where $\langle \Delta_{41} \rangle$ is the mean three-photon detuning. At this point we make an assumption that the transition frequencies ω_{31} and ω_{32} undergo identical fluctuations, i.e., $\delta_{31} = \delta_{32}$, and $\delta_{42} = \delta_{41}$. We then use $\Delta_{41} \equiv \langle \Delta_{41} \rangle + \delta_{41}$, with $\Delta_{21} = \omega_p - \omega_c - \omega_{21}$ being a deterministic quantity.

We further assume that the random energy shifts δ_{31} and δ_{41} are distributed according to the Lorentzian function: $P(\delta_{31}) = (1/\pi)\sigma_3/(\delta_{31}^2 + \sigma_3^2)$ and $P(\delta_{41}) = (1/\pi)\sigma_4/(\delta_{41}^2 + \sigma_4^2)$. Under these assumptions, we can obtain the disorder-averaged susceptibility from the integral

$$\begin{aligned} \langle \chi_p \rangle &= \int_{-\infty}^{\infty} d\delta_{31} \int_{-\infty}^{\infty} d\delta_{41} [\chi_p(\delta_{31}, \delta_{41}) P(\delta_{31}) P(\delta_{41})] \\ &= K \frac{\sigma_3 \sigma_4}{\pi^2} \int_{-\infty}^{\infty} \int_{-\infty}^{\infty} \frac{d\delta_{31} d\delta_{41}}{[\delta_{31}^2 + \sigma_3^2][\delta_{41}^2 + \sigma_4^2]} \times \frac{D_{21}(D_{41} + \delta_{41}) - \Omega_s^2}{D_{21}(D_{31} + \delta_{31})(D_{41} + \delta_{41}) - \Omega_s^2(D_{31} + \delta_{31}) - \Omega_c^2(D_{41} + \delta_{41})}, \end{aligned} \quad (\text{C1})$$

where we have defined the complex detunings $D_{21} \equiv \langle \Delta_{21} \rangle + i\gamma_{21}$, $D_{31} = \langle \Delta_{31} \rangle + i\gamma_{31}$ and $D_{41} = \langle \Delta_{41} \rangle + i\gamma_{41}$. Carrying out the double contour integration in Eq. (C1), we obtain the following result:

$$\langle \chi_p \rangle_E = \frac{K}{(\Delta_{31} + I'_E) + i(\Sigma_{31} + I''_E)}, \quad (\text{C2})$$

where the complex quantity $I_E = I'_E + iI''_E$, can be written as

$$I_E = \frac{\Omega_c^2(\Delta_{41} + i\Sigma_{41})}{\Omega_s^2 - (\Delta_{21} + i\gamma_{21})(\Delta_{41} + i\Sigma_{41})}. \quad (\text{C3})$$

with $\Sigma_{31} = \gamma_{31} + \sigma_3$, and $\Sigma_{41} = \gamma_{41} + \sigma_4$, as before. The disorder-averaged equations (C2) and (C3) differ from the homogeneous equations (A9) and (A11) only by the magnitude of the broadenings, which now account for the disorder.

Appendix D: Optimal nonlinear coherent signals for photoswitches with energy disorder

As discussed in the main text, we characterize the nonlinear signal coherence by the figure-of-merit $\eta = \text{Re}[\chi_p]/(2\text{Im}[\chi_p])$. Detectible coherent (dispersive) signals require $\eta > 1$. Our goal is to understand whether η can still exceed unity in the presence of energy disorder for an intracavity photoswitch medium.

1. Figure-of-merit in the absence of the signal field: Pure VIT regime

In the absence of the signal field ($\Omega_s = 0$), we focus on the properties of $\eta_{\text{VIT}} = \text{Re}[\chi_p^{\text{VIT}}]/(2\text{Im}[\chi_p^{\text{VIT}}])$, with χ_p^{VIT} given by the disorder-free expression in Eq. (A14). η_{VIT} clearly does not characterize the nonlinear phase shift of the probe in the presence of the signal field, but can still be considered to quantify the probe coherence under conditions of VIT. Extracting $\text{Re}[\chi_p^{\text{VIT}}]$ and $\text{Im}[\chi_p^{\text{VIT}}]$ from Eq.(A14) we obtain

$$\eta_{\text{VIT}} = -\frac{\Delta_{31} - \lambda_c \Delta_{21}}{2(\gamma_{31} + \lambda_c \gamma_{21})}. \quad (\text{D1})$$

We denote the probe detuning as $\Delta_{31} \equiv x$, assume that the cavity is on resonance with the $|2\rangle \rightarrow |3\rangle$ transition, so that $\Delta_{21} = x$, and use the definition of the cavity parameter $\lambda_c(x) = \Omega_c^2/(x^2 + \gamma_{21}^2)$ (A13) to rewrite the equation for η_{VIT} in the form

$$\eta_{\text{VIT}}(x) = -\frac{x(x^2 + \gamma_{21}^2) - \Omega_c^2 x}{2[\gamma_{31}(x^2 + \gamma_{21}^2) + \gamma_{21}\Omega_c^2]}. \quad (\text{D2})$$

In the absence of the cavity field ($\Omega_c = 0$), we have $\eta_{\text{free space}}(x) = -x/2\gamma_{31} \ll 1$ for $x \ll \gamma_{31}$. Inspection of Eq. (D2) reveals that the VIT enhancement, i.e. $\eta_{\text{VIT}} > 1$, can be reached only when γ_{21} is very small compared to γ_{31} , and x is at most of the order of $\Omega_c \sqrt{\gamma_{21}/\gamma_{31}}$. Assuming the hierarchy of the energy scales $\gamma_{21} \ll x \ll \Omega_c, \gamma_{31}$, we can write

$$\eta_{\text{VIT}}(x) \approx \frac{\Omega_c^2 x}{2[\gamma_{31}x^2 + \gamma_{21}\Omega_c^2]} \sim O\left(\frac{x}{\gamma_{21}}\right) \gg 1. \quad (\text{D3})$$

This function has a maximum at the optimal probe detuning $x_* = \Omega_c \sqrt{\gamma_{21}/\gamma_{31}}$. Substituting x_* into Eq. (D3) gives an optimal figure-of-merit for the disorder-free case of the form

$$\eta_{\text{VIT}}^{\text{max}} = \frac{\Omega_c}{4\sqrt{\gamma_{21}\gamma_{31}}}. \quad (\text{D4})$$

The *disorder averaged* optimal figure-of-merit can be obtained within our Lorentzian disorder ansatz by simply replacing γ_{31} with $\Sigma_{31} \equiv \gamma_{31} + \sigma_3$ from Eq. (D4), to read

$$\langle \eta_{\text{VIT}}^{\text{max}} \rangle = \frac{\Omega_c}{4\sqrt{\gamma_{21}\Sigma_{31}}}. \quad (\text{D5})$$

2. Figure-of-merit in the presence of the signal field: VIT-Kerr regime

Starting with the disorder-free susceptibility χ_p in Eq. (A9) and I_0 in Eq. (A11), we can write the figure-of-merit η as

$$\eta = -\frac{\Delta_{31} - \frac{\Omega_c^2(\Delta_{21} - \lambda_s \Delta_{41})}{(\Delta_{21} - \lambda_s \Delta_{41})^2 + (\gamma_{21} + \lambda_s \gamma_{41})^2}}{2\left[\gamma_{31} + \frac{\Omega_c^2(\gamma_{21} + \lambda_s \gamma_{41})}{(\Delta_{21} - \lambda_s \Delta_{41})^2 + (\gamma_{21} + \lambda_s \gamma_{41})^2}\right]}, \quad (\text{D6})$$

where we have defined the dimensionless signal parameter $\lambda_s = \Omega_s^2/(\Delta_{41}^2 + \gamma_{41}^2)$. As required for consistency, Eq. (D6) reduces to η_{VIT} in Eq. (D1), in the limit $\lambda_s \rightarrow 0$.

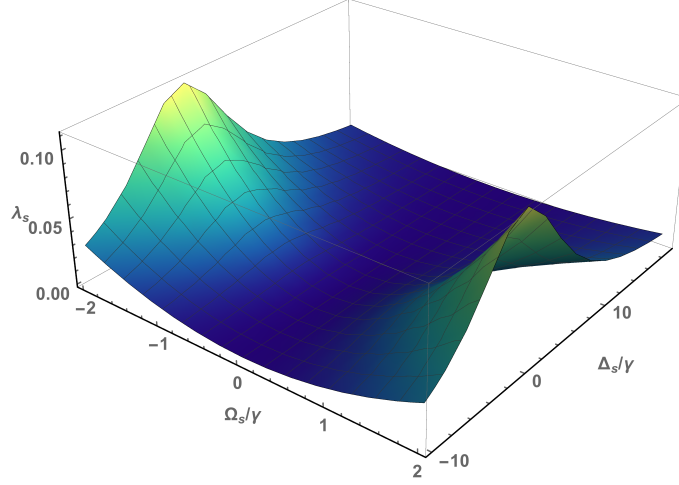


FIG. D.1: Signal parameter λ_s as a function of signal detuning Δ_s/γ and Rabi frequency Ω_s/γ , for $\Sigma_{41} = 6\gamma$.

In order to understand the scaling of the *disorder-averaged* figure-of-merit $\langle \eta \rangle$ with the characteristic variables of the signal field (Ω_s, Δ_s) , we first rewrite Eq. (D6) using $x \equiv \Delta_{31}$, $\Delta_{21} = x$, and $\Delta_{41} = x + \Delta_s$, where $\Delta_s = \omega_s - \langle \omega_{42} \rangle$. Assuming that $|x| \ll |\Delta_s|$. We define the dimensionless x -independent signal parameter

$$\lambda_s = \frac{\Omega_s^2}{\Delta_s^2 + \gamma_{41}^2}. \quad (\text{D7})$$

Finally, within our Lorentzian disorder model, we make the substitutions $\gamma_{31} \rightarrow \Sigma_{31} \equiv \gamma_{31} + \sigma_3$ and $\gamma_{41} \rightarrow \Sigma_{41} \equiv \gamma_{41} + \sigma_4$ in Eq. (D6) to obtain a mean figure-of-merit in the form

$$\langle \eta(x) \rangle = -\frac{x[(x - x_s)^2 + (\gamma_{21} + \gamma_s)^2] - \Omega_c^2(x - x_s)}{2\{\Sigma_{31}[(x - x_s)^2 + (\gamma_{21} + \gamma_s)^2] + (\gamma_{21} + \gamma_s)\Omega_c^2\}}, \quad (\text{D8})$$

where we have introduced the shift parameter x_s and the linewidth parameter γ_s , defined as

$$x_s \equiv \lambda_s \Delta_s = \frac{\Omega_s^2 \Delta_s}{\Delta_s^2 + \Sigma_{41}^2} \quad \text{and} \quad \gamma_s \equiv \lambda_s \Sigma_{41} = \frac{\Omega_s^2 \Sigma_{41}}{\Delta_s^2 + \Sigma_{41}^2}. \quad (\text{D9})$$

The comparison of Eq. (D8) with Eq. (D2) reveals that in the presence of the signal field, the figure-of-merit $\langle \eta \rangle$ has the same functional form as in the case where no signal field is present (pure VIT). The net effect of the signal field is to blue-shift the optimal probe frequency by x_s (for $\Delta_s \geq 0$) and broaden the $\eta(x)$ -profile by γ_s . We can thus follow the same analysis as before, to show that the mean figure-of-merit $\langle \eta(x) \rangle$ in the presence of the signal field, is upper bounded by $\langle \eta_{\text{VIT}}^{\text{max}} \rangle = \Omega_c / (4\sqrt{\gamma_{21}\Sigma_{31}})$.

Finally, the similarity between the VIT and Kerr schemes shows that large values of the figure-of-merit $\langle \eta \rangle$ can be obtained under the conditions $\gamma_s \leq \gamma_{21}$ and $|x_s| \leq x_* \equiv \Omega_c \sqrt{\gamma_{21}/\Sigma_{31}}$, which can be summarized into the *signal field* parameter bound

$$\frac{\Omega_s^2}{\Delta_s^2 + \Sigma_{41}^2} \leq \frac{\gamma_{21}}{\Sigma_{41}}, \quad \text{and} \quad \frac{\Omega_s^2 |\Delta_s|}{\Delta_s^2 + \Sigma_{41}^2} \leq \Omega_c \sqrt{\frac{\gamma_{21}}{\Sigma_{31}}}. \quad (\text{D10})$$

which reduce into the single constraint in Eq. (6) of the main text, when assuming that with $\Sigma_{41} \approx \Sigma_{31} \approx \sigma$ and $\Omega_c/|\Delta_s| \leq \sqrt{\gamma_{21}/\sigma}$. As Fig. D.1 illustrates (σ_4 fixed), high VIT coherence for the Kerr nonlinearity ($\lambda_s \ll 1$) can be reached by either:

- Decreasing Ω_s , effectively switching the signal off. The signal field party destroys VIT, as it is not protected by the transparency window.
- Increasing Δ_s , making the incoherent signal field less resonant and therefore less absorptive.

- Increasing σ_4 , effectively distributing the signal beam among many frequencies, many of which are far-detuned from $\langle\omega_{24}\rangle$ and therefore less absorptive.

- (1) J. Gea-Banacloche, Y.-Q. Li, S.-Z. Jin, and M. Xiao, Phys. Rev. A 51, 576, 1995.
 - (2) A. Javan, O. Kocharovskaya, H. Lee, and M. Scully, Physical Review A 66, 013805, 2002.
-